Nano Energy 61 (2019) 111–118

Contents lists available at ScienceDirect

Nano Energy

journal homepage: www.elsevier.com/locate/nanoen

Full paper

Remarkable merits of triboelectric nanogenerator than electromagnetic generator for harvesting small-amplitude mechanical energy

Junqing Zhao[a,c,1], Gaowei Zhen[a,b,1], Guoxu Liu[a,c], Tianzhao Bu[a,c], Wenbo Liu[a], Xianpeng Fu[a], Ping Zhang[b,**], Chi Zhang[a,c,d,*], Zhong Lin Wang[a,c,d,e,***]

[a] CAS Center for Excellence in Nanoscience, Beijing Key Laboratory of Micro-nano Energy and Sensor, Beijing Institute of Nanoenergy and Nanosystems, Chinese Academy of Sciences, Beijing, 100083, PR China
[b] School of Electrical and Information Engineering, Tianjin University, Tianjin, 300072, China
[c] School of Nanoscience and Technology, University of Chinese Academy of Sciences, Beijing, 100049, PR China
[d] Center on Nanoenergy Research, School of Physical Science and Technology, Guangxi University, Nanning, 530004, China
[e] School of Material Science and Engineering Georgia Institute of Technology, Atlanta, GA, 30332, USA

ARTICLE INFO

Keywords:
Triboelectric nanogenerator
Electromagnetic generator
Small-amplitude
Mechanical energy
Energy harvesting

ABSTRACT

Triboelectric nanogenerator (TENG) is a new energy technology that is as important as traditional electromagnetic generator (EMG) for converting mechanical energy into electricity, which shows great advantages of simple structure, high power density and low-frequency. Here, the effects of motion amplitude for both generators are first taken into consideration. Our result demonstrates that the TENG has a much better performance than that of the EMG at small amplitude. Under fixed operation frequency, the maximum output power of the TENG rapidly grows to saturation with the increase of the amplitude, while that of the EMG grows slowly and gradually. This contrastive characteristic is verified at different frequencies, which has demonstrated that the TENG has dominant scope over the EMG, in not only low-frequency but also small-amplitude. Moreover, electronics powered by the TENG in small-amplitude has been exhibited and an overall comparison of the TENG and EMG is summarized. Beyond low-frequency, this work has verified the small-amplitude is also a remarkable merit of the TENG for harvesting micro-mechanical energy, which has guided the development prospects of TENG as a foundation of the energy for the new era for internet of things, wearable electronics, robotics and artificial intelligence.

1. Introduction

Electronics is developing toward miniaturized integration, functionality and wireless portability [1,2]. With the increasing demands for self-powering in the Internet of Things era [3–6], the eco-friendly and sustainable energy supply for millions of sensors has become a major issue that should be addressed urgently [7,8]. Nowadays, harvesting ambient mechanical energy by triboelectric nanogenerator (TENG) for power generation has attracted growing attentions for the great advantages such as simple-structure [9–12], high power density [13,14] and wide selection of materials [15,16]. Derived from the second term in Maxwell's displacement current [17–19], the TENG has been widely used in micro/nano power sources [20–23], self-powered sensing [24–30], blue energy [31–35], and high voltage sources [36–40] since invented in 2012.

As a new energy technology, the TENG has demonstrated comparability and symmetry with the traditional electromagnetic generator (EMG) in working mechanisms, governing equations, and output characteristics [41]. The TENG can be considered as a current source with a large internal resistance, while the EMG is close to a voltage source with a small internal resistance. With the complementary application prospects, the TENG could be equivalently important as the EMG for harvesting mechanical energy. Moreover, the TENG has shown a much better performance than that of the EMG at low frequency (typically < 5 Hz), which indicates a great advantage and possible killer applications of TENG in low-frequency mechanical energy harvesting, such as human motions and ocean waves in our living environment [42]. However, the mechanical energy sources have

* Corresponding author. Beijing Institute of Nanoenergy and Nanosystems, Chinese Academy of Sciences, Beijing 100083, China.
** Corresponding author. Beijing Institute of Nanoenergy and Nanosystems, Chinese Academy of Sciences, Beijing 100083, China.
*** Corresponding author. Beijing Institute of Nanoenergy and Nanosystems, Chinese Academy of Sciences, Beijing 100083, China.
E-mail addresses: zhangping@tju.edu.cn (P. Zhang), czhang@binn.cas.cn (C. Zhang), zlwang@gatech.edu (Z.L. Wang).
[1] These authors contributed equally to this work.

https://doi.org/10.1016/j.nanoen.2019.04.047
Received 20 March 2019; Received in revised form 11 April 2019; Accepted 11 April 2019
Available online 15 April 2019

different motion amplitudes and some of them are very small, such as slight vibration [43–45]. Comprehensively considering the frequency and amplitude in mechanical energy harvesting, it is advisable to study the effects of motion amplitude for both generators and reveal the dominant scope of the TENG in both frequency and amplitude.

Here in this work, the effects of motion amplitude for both generators are first taken into consideration, which demonstrates that the TENG has a much better performance than that of the EMG at smaller amplitude. Under fixed operation frequency, the maximum output power of the TENG rapidly grows to saturation with the increase of the amplitude, while that of the EMG grows slowly and gradually. This contrastive characteristic is verified at different frequencies, which has demonstrated that the TENG has dominant scope over the EMG, in not only low-frequency but also small-amplitude. Moreover, electronics powered by the TENG in small-amplitude has been exhibited and an overall comparison of the TENG and EMG is summarized. Beyond low-frequency, this work has verified the small-amplitude is also a remarkable merit of the TENG for harvesting micro-mechanical energy, which has guided the development prospects of TENG as a foundation of the energy for the new era, the era of internet of things, wearable electronics, robotics and artificial intelligence.

2. Results and discussion

Fig. 1 illustrates the 3D schematics, photos and working principles of the fabricated EMG and TENG in both contact-separation mode and keeps their sizes the same. The EMG has the structure of a piece of square magnet and a copper (Cu) coil sandwiched in two acrylic sheets, as shown in Fig. 1a. While the TENG mainly consists of a top Cu film and a fluorinated ethylene propylene (FEP) film with a bottom Cu film on the back, as shown in Fig. 1b. The fabrication processes of the two generators are described in details in the Experimental Methods section. Fig. 1c illustrates the working principle of the EMG. According to Faraday's law of electromagnetic induction, when the magnet moves away from the Cu coil by an external mechanical excitation, the magnetic flux through the Cu coil will be changed, resulting in an electrodynamic potential and thus a current in the closed loop. An opposite current will be generated in the closed loop when the magnet moves back to the original position. Thus, an alternating current can be generated with the reciprocating motion of the magnet. While derived from the second term in Maxwell's displacement current, the TENG shows a different working principle from the EMG. As shown in Fig. 1d, equal opposite charges can be created on the surfaces of Cu film and FEP film by a fully contact between them, with no electrons flowing for the electrostatic balance. When the Cu film gradually separates from the FEP film by an external mechanical excitation, free electrons are driven to flow from the bottom Cu electrode to the top one by the potential difference. When the Cu film moves back, the electrons flow back to reach the electrostatic balance state again, producing an opposite current. With the reciprocating motion of the top Cu film, an alternating current can also be generated.

We first give a theoretical comparison of the EMG and TENG in their open-circuit voltage and short-circuit current. For the EMG, we assume the intensity of magnetic field produced by the magnet remains nearly

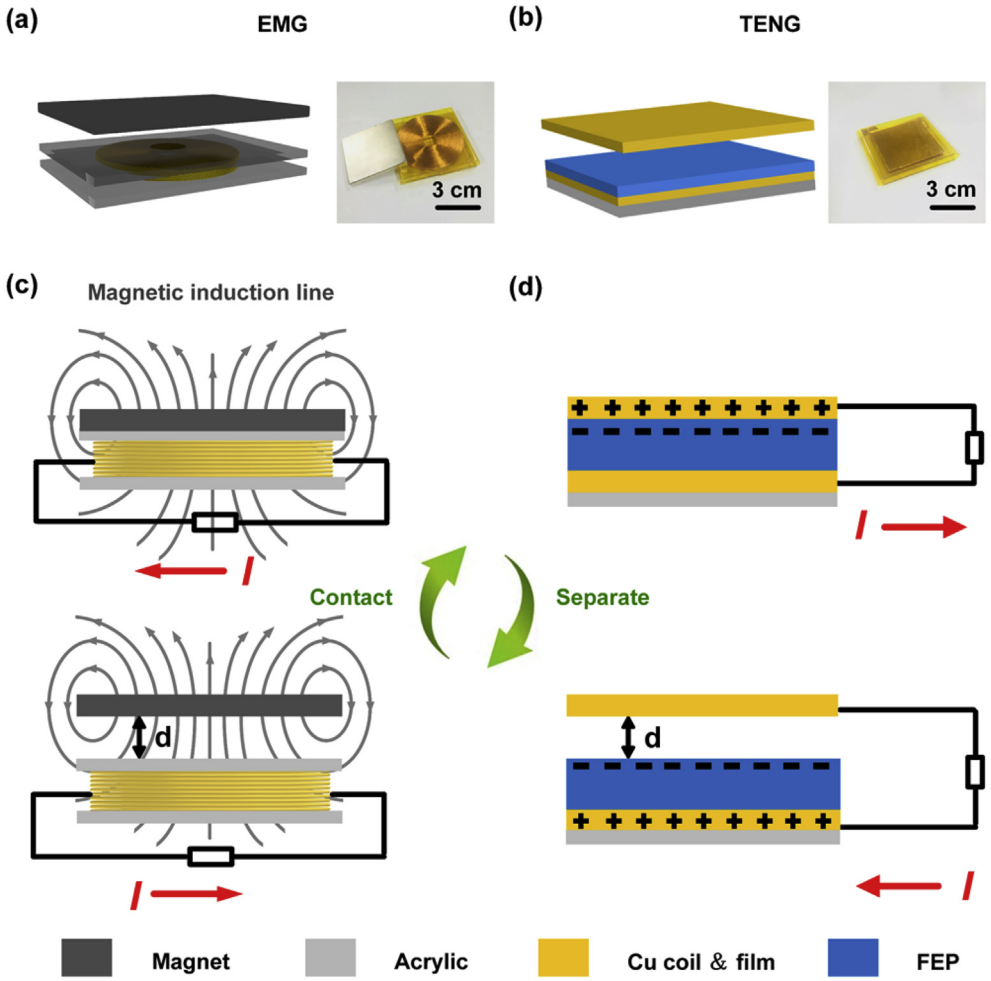

Fig. 1. Schematic illustrations and working principles of both fabricated generators. 3D schematics, photos of fabricated (a) EMG and (b) TENG. Working principles of (c) EMG and (d) TENG.

constant at small displacement, so the open-circuit voltage and short-circuit current can be expressed as:

$$V_{OC}^{EMG}(t) = B{\cdot}l{\cdot}v(t) \tag{1}$$

$$I_{SC}^{EMG}(t) = \frac{V_{OC}^{EMG}(t)}{r} = \frac{B{\cdot}l{\cdot}v(t)}{r} \tag{2}$$

Where B is the intensity of magnetic field, l is the total lengths of the coil, $v(t)$ is the moving velocity of the magnet that varies with time t, and r is the coil's inner resistance.

From the above eqs (1) and (2), we notice that the open-circuit voltage and short-circuit are both proportional to the motion velocity. Specially, for a simple harmonic motion, the motion displacement and velocity can be described as:

$$x(t) = x_{\max}\sin(2\pi \mathrm{ft}) \tag{3}$$

$$v(t) = \frac{\mathrm{d}x}{\mathrm{d}t} = 2\pi \mathrm{f}x_{\max}\cos(2\pi \mathrm{ft}) \tag{4}$$

Here, $x_{\max}$ is the motion amplitude. The open-circuit voltage and short-circuit current of the EMG at different displacement can be derived as:

$$V_{OC}^{EMG}(t) = 2\pi Blfx_{\max}\cos(2\pi \mathrm{ft}) \tag{5}$$

$$I_{SC}^{EMG}(t) = \frac{2\pi Blfx_{\max}\cos(2\pi \mathrm{ft})}{r} \tag{6}$$

Therefore, the maximum open-circuit voltage and short-circuit current of the EMG is:

$$V_{OC,\max}^{EMG} = 2\pi B\mathrm{l}\mathrm{f}x_{\max} \tag{7}$$

$$I_{SC,\max}^{EMG} = \frac{2\pi Blfx_{\max}}{r} \tag{8}$$

From eqs (7) and (8), we notice that, when the frequency f remains constant, the maximum open-circuit voltage and short-circuit current are both proportional to the motion amplitude $x_{\max}$. Fig. 2a and b demonstrate the experimental results that the maximum open-circuit voltage and short-circuit current of the EMG have both linear relationships with the amplitude in range of 3 mm at different frequency from 0.5 to 8 Hz, which are consistent with the theoretical derivation above.

Unlike the EMG, the TENG shows much different characteristics in open-circuit voltage and short-circuit current. At the small displacement, the triboelectric surface area of TENG is much larger than the separation distance. According to the previous reports [46,47], the open-circuit voltage can be calculated as following:

$$C(x) = \frac{\varepsilon_0 S}{d_0 + x(\mathrm{t})} \tag{9}$$

$$Q_{SC}(x) = \frac{S\sigma \mathrm{x}(t)}{d_0 + x(t)} \tag{10}$$

$$V_{OC}^{TENG}(t) = \frac{Q_{SC}(x)}{C(x)} = \frac{\sigma x(t)}{\varepsilon_0} \tag{11}$$

where $C(x)$ is the capacitance between two electrodes subject to various displacement x, ε_0 is the permittivity of vacuum, S is the triboelectric surface area, d_0 is the effective thickness of the dielectric layer, σ is the triboelectric surface charge density, and Q_{SC} (x) is the short-circuit charge transfer amount subject to the displacement x. From eq (11), we can observe that the open-circuit voltage of the TENG is independent of the frequency f, and only increases with the larger displacement. The maximum open-circuit voltage can be reached when the displacement x increases to the amplitude $x_{\max}$, which is described as:

$$V_{OC,\max}^{TENG} = \frac{\sigma x_{\max}}{\varepsilon_0} \tag{12}$$

Eq (12) demonstrates that the maximum open-circuit voltage of the TENG is proportional to $x_{\max}$ at small amplitude. While the amplitude is sufficiently large, the assumption that the electrodes area of the TENG is infinitely large will be untenable, leading to the open-circuit voltage deviates from the linear relationship with the amplitude due to the edge effect. Fig. 2c shows that the measured maximum open-circuit voltage of the TENG increases with the increasing amplitude $x_{\max}$ linearly at first and then slowly reaches to saturation in the range of 3 mm. In particular, the frequency makes nearly no impact on the characteristic curves, which is in agreement with the theoretical analysis above and much different from the characteristic of EMG. Besides, the short-circuit current of the TENG is given by [47].

$$I_{SC}^{TENG}(t) = \frac{\mathrm{d}Q_{SC}(x)}{\mathrm{d}t} = \frac{S\sigma d_0}{(d_0 + x(t))^2}\frac{\mathrm{d}x}{\mathrm{d}t} = \frac{S\sigma d_0 v(t)}{(d_0 + x(t))^2} \tag{13}$$

According to eq (13), the maximum short-circuit current when $x(t) = 0$ can be defined as:

$$I_{SC,\max}^{TENG} = \frac{S\sigma v(t)}{d_0} = \frac{2\pi S\sigma x_{\max} f\cos(2\pi \mathrm{ft})}{d_0} = \frac{2\pi S\sigma f x_{\max}}{d_0} \tag{14}$$

Therefore, the maximum short-circuit current is proportional to the amplitude $x_{\max}$ when the frequency f keeps constant. Fig. 2d shows that the measured maximum short-circuit current of the TENG linearly increases with the larger amplitude in the range of 3 mm at different frequency from 0.5 to 8 Hz, which is consistent with the discussion above and similar to the characteristic of EMG.

To evaluate the output capability of the EMG and TENG, we have compared the average output power of both generators. Generally, the output power of the EMG can be calculated as following:

$$P^{EMG} = \left(\frac{V_{OC}^{EMG}}{\mathrm{r}+R}\right)^2 R \tag{15}$$

Where R is the external resistance. The maximum output power is given when $R = r$, so the maximum average output power in one cycle is:

$$\overline{P_{\max}^{EMG}} = \frac{\overline{(V_{OC}^{EMG})^2}}{4r} = \frac{\int_0^T (V_{OC}^{EMG})^2 \mathrm{d}t}{4Tr} = \frac{(\pi fBl)^2}{2r}(x_{\max})^2 \tag{16}$$

Therefore, the maximum average output power of the EMG is proportional to the square of the amplitude when the frequency f remains constant.

For the TENG, the theoretical maximum average output power can be calculated as:

$$\overline{P_{\max,\mathrm{CMEO}}^{TENG}} = \frac{E_{\max}}{T} = E_{\max} f \tag{17}$$

Where $E_{\max}$ is the theoretical maximum output energy per cycle. According to the cycle of maximized energy output (CMEO), $E_{\max}$ can be described as [48].

$$E_{\max} = \frac{1}{2}Q_{SC,\max}(V_{OC,\max}^{TENG} + V'_{\max}) \tag{18}$$

Where V'_{max} is the maximum achievable absolute voltage when $Q_{SC} = Q_{SC,\ max}$. For the TENG in contact-separation mode, the V'_{max} is defined as [46].

$$V'_{\max} = \frac{Q_{SC,\max}}{C_2} = \frac{Q_{\mathrm{SC},\max}}{\varepsilon_0 S/d_0} = \frac{d_0 Q_{SC,\max}}{\varepsilon_0 S} \tag{19}$$

Where C_2 is the capacitance between the top surface of dielectric and the bottom electrode of the TENG. Therefore, the theoretical maximum average output power is calculated as:

$$\overline{P_{\max,\mathrm{CMEO}}^{TENG}} = \frac{1}{2}Q_{SC,\max}\left(V_{OC,\max}^{TENG} + \frac{d_0 Q_{SC,\max}}{\varepsilon_0 S}\right)\mathrm{f} \tag{20}$$

From eq (20), we can observe that, when the frequency f keeps

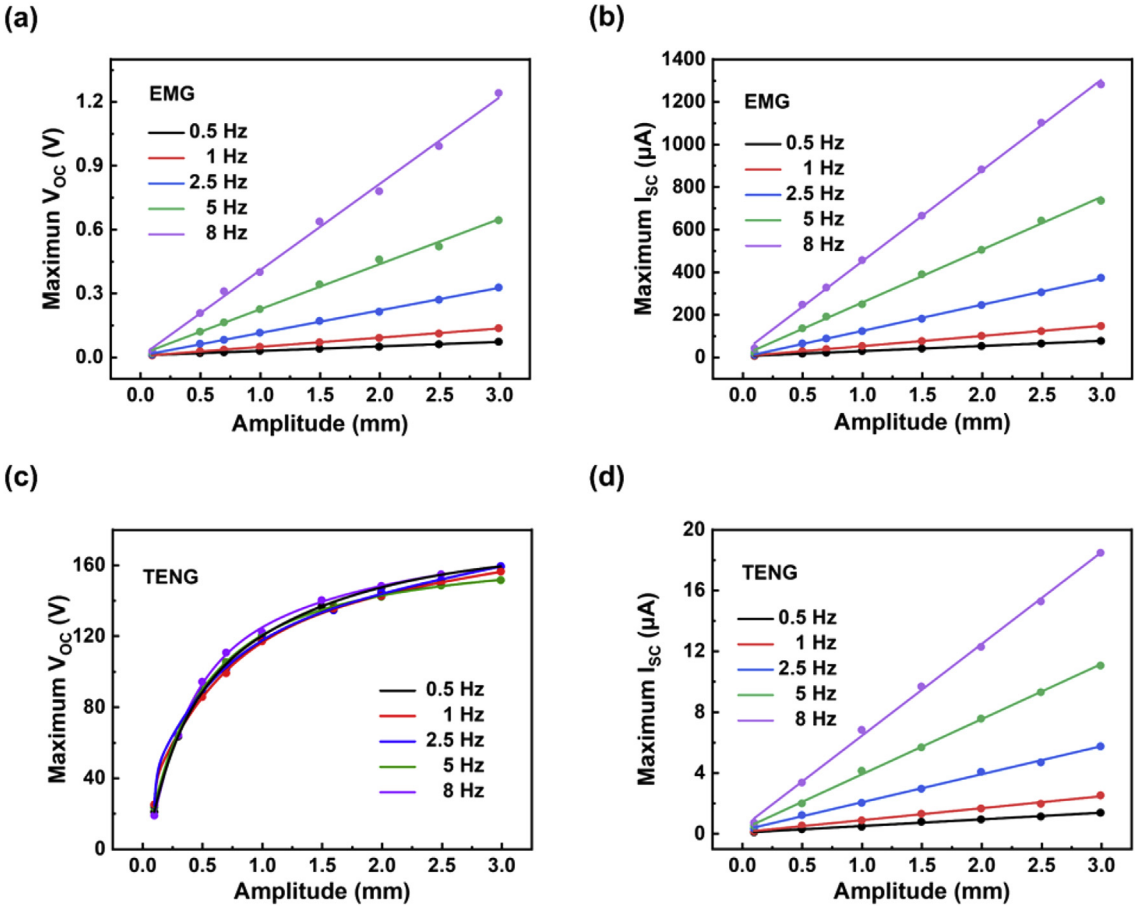

Fig. 2. Maximum open-circuit voltage and short-circuit current comparison of both generators versus amplitude at different fixed frequencies. (a) Measured maximum open-circuit voltages and (b) short-circuit currents of the EMG versus amplitude at different frequency. (c) Measured maximum open-circuit voltages and (d) short-circuit currents of the TENG versus amplitude at different frequency.

constant, the theoretical maximum average output power is determined by the maximum short-circuit transferred charges and maximum open-circuit voltage. As shown in eq (10), the maximum short-circuit transferred charge is kept at $x = x_{max}$,

$$Q_{SC,max} = \frac{S\sigma x_{max}}{d_0 + x_{max}} = \frac{S\sigma}{(d_0/x_{max}) + 1} \tag{21}$$

It is clearly observed that the maximum short-circuit transferred charge increases with the amplitude x_{max} at small amplitude. However, when amplitude x_{max} is sufficiently large, no charge will transfer between the electrodes in a saturation state for the too small capacitance [46]. Fig. S1 shows that the measured maximum short-circuit transfer charge of the TENG increases with the increasing amplitude linearly at first and then slowly reaches to saturation in the range of 3 mm, agreeing well with the theoretical analysis and similar to the maximum open-circuit voltage characteristic of TENG. Therefore, the theoretical maximum average output power of the TENG versus amplitude could increase at first and then approach to saturation. The output power versus external load can be calculated as:

$$\overline{P^{TENG}} = \frac{\int_0^T V^2 dt}{RT} \tag{22}$$

Where V is the voltage of the external resistance. For an approximate calculation, the average output power at the matched external could be equivalent to the half of the theoretical maximum average output power, which could have similar variation trend versus amplitude.

Fig. 3a and b exhibit the measured average output power versus external resistance with different amplitude at 1 Hz for the EMG and TENG, respectively. We plot the maximum average output power at each amplitude x_{max} for both generators. As shown in Fig. 3c, the maximum average output power of the TENG rapidly grows and remains virtually constant after 1.5 mm. While the maximum average output power of the EMG grows slowly and gradually, crossing with the curve of TENG at 2.6 mm. The experimental results show a consistency with the discussion above and demonstrate that the TENG has a much better performance than that of the EMG within 2.6 mm at 1 Hz. Furthermore, at different frequency from 0.5 to 8 Hz, the average output power versus external resistance for the EMG and TENG are shown in Figs. S2 and S3, respectively. At each frequency, the maximum average output power versus amplitude for both generators are plotted in Fig. S4. We can observe that the both maximum average output powers versus amplitude show similar trends and characteristics at different frequency. These results indicate that the TENG is superior to the EMG with remarkable merits for harvesting mechanical energy in small amplitude.

Meanwhile, the amplitudes in crossover points of both maximum average output power characteristic curves at different frequency are summarized in Fig. 3d. The results illustrate that the amplitude in crossover point decreases with the increasing frequency. Beneath the fitted line, the light red area denotes the dominant scope of TENG while the light green area denotes that of EMG. The lower the frequency, the larger the advantage scope of TENG at small-amplitude, demonstrating that the TENG has dominant scope over the EMG, in not only low-frequency but also small amplitude. As an alternative demonstration, the maximum accelerations in crossover points of maximum average output

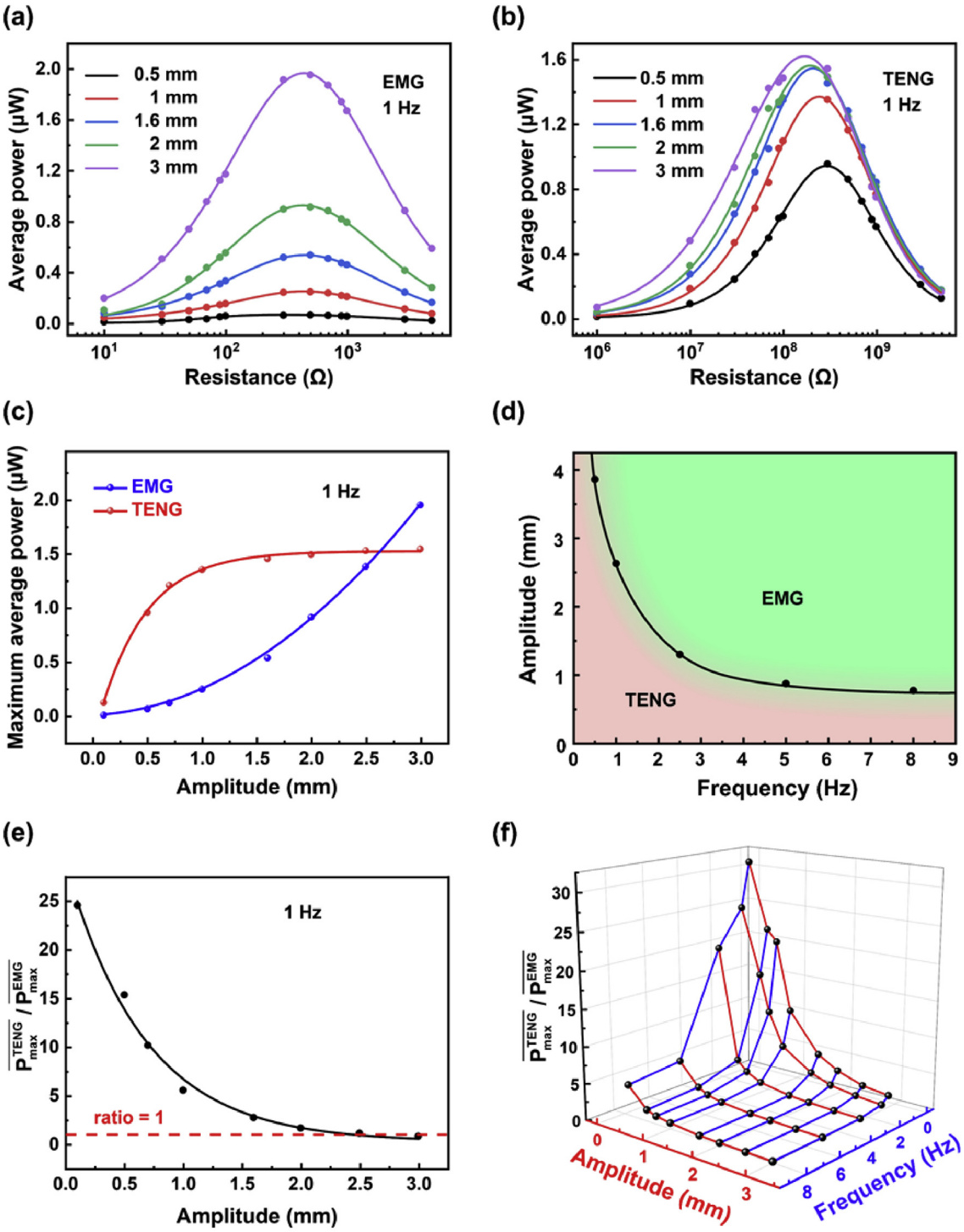

Fig. 3. Average output power comparison of both generators with different amplitude and operation frequency. Impedance matchings of the (a) EMG and (b) TENG with different amplitudes at 1 Hz. (c) Maximum average power comparison of both generators versus amplitude at 1 Hz. (d) Amplitudes in crossover points of two characteristic curves at different frequencies. The light red area denotes the dominant scope of TENG in low-frequency and small-amplitude while the light green area denotes that of EMG. (e) Maximum average output power ratio of TENG and EMG versus amplitude at 1 Hz. (f) Maximum average output power ratio of TENG and EMG versus amplitude and frequency. (For interpretation of the references to colour in this figure legend, the reader is referred to the Web version of this article.)

power characteristic curves for both generators at different frequency are also exhibited in Fig. S5. It indicates that, even at a higher frequency, the TENG also has a dominant scope over the EMG at small acceleration, which is more suitable for vibration energy harvesting with low impact. The maximum acceleration can be calculated as following:

$$a = \frac{dv}{dt} = -4x_{max}\pi^2 f^2 \sin(2\pi ft) \tag{23}$$

$$|a_{max}| = 4x_{max}\pi^2 f^2 \tag{24}$$

As shown in Fig. 3e, we also plot the maximum average output power ratio for the TENG and EMG versus amplitude in the range of 3 mm at 1 Hz, which has shown that the ratio decreases with the

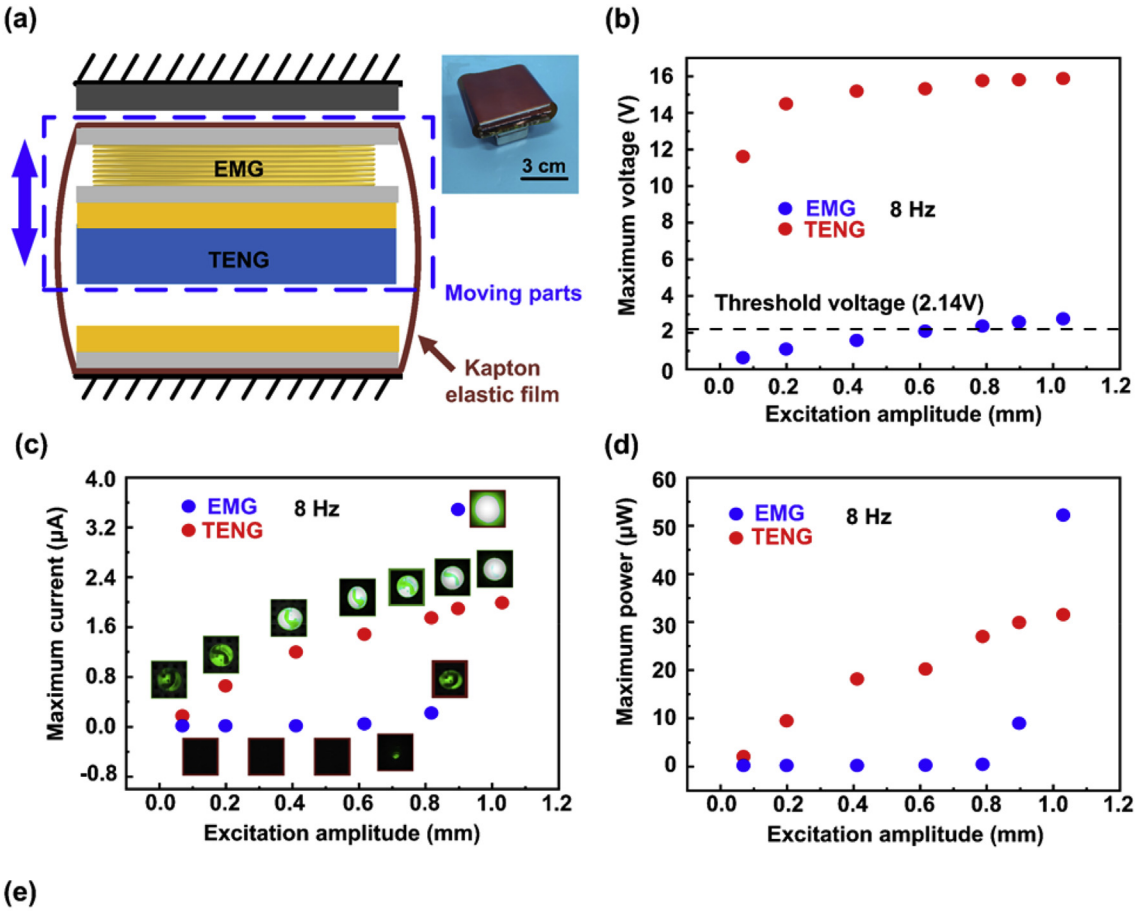

(e)

	EMG	TENG
Approximate equivalence	Voltage Source	Current Source
Internal impedance	Small	Large
Impedance characteristic	Resistive, inductive	Capacitive
Open-circuit voltage	Low	High
Short-circuit voltage	High	Low
Frequency	High	Low
Amplitude	Large	Small

Fig. 4. Demonstration and summary of TENG. (a) Schematic and photograph of the integration of EMG and TENG. (b) Maximum voltage of an LED versus excitation amplitude at 8 Hz driven by the EMG and TENG. (c) Maximum current through an LED versus excitation amplitude at 8 Hz as driven by the EMG and TENG, respectively, with photos of the lighting LED for a visual indication of the generated power. (d) Maximum power of an LED versus excitation amplitude at 8 Hz driven by the EMG and TENG. (e) Summarized overall comparison of EMG and TENG.

increasing amplitude, demonstrating that the advantage of the TENG over the EMG is greater with smaller amplitude within 2.6 mm. The maximum average output power ratio of TENG and EMG versus amplitude and frequency are also summarized in Fig. 3f. The result shows that the ratio decreases with the increasing amplitude and frequency. The smaller the amplitude and frequency, the larger advantage of the TENG over the EMG.

To demonstrate the merit of the TENG for vibration energy harvesting in small amplitude, a hybrid structure referred previous work [49,50]by integrating the EMG and TENG are designed and fabricated, in which the two generators can work at the same amplitude and frequency, as shown in Fig. 4a. Fig. 4b illustrates the maximum voltage of the LEDs lighted by the EMG and TENG with different amplitude at 8 Hz. We can observe that the voltage of the LEDs driven by the TENG is higher than the threshold voltage (2.14 V) of the LEDs at small amplitude, while that of the EMG grows slowly and cannot increase over the threshold voltage of the LEDs until 0.7 mm. The maximum current and power of the LEDs lighted by the EMG and TENG with different amplitude at 8 Hz are demonstrated in Fig. 4c and d, respectively. The results indicate that, the maximum current and power of the LEDs lighted by the TENG both rapidly grow to saturation. While for the EMG, the maximum current and power both grow slowly, and exceed those of TENG after 0.87 mm and 1 mm, respectively. As a visual demonstration, the luminance of the LEDs lighted by the EMG and TENG are inserted in the current curves in Fig. 4c. It shows that the LEDs can be lighted by the TENG at the amplitude less than 0.1 mm, and the brightness rapidly grows to saturation around 1 mm. While the LEDs cannot be lighted by the EMG until 0.7 mm, and then the brightness sharply increases and exceeds that of TENG after 0.87 mm, which has visually indicated the advantage over the EMG in small amplitude. The

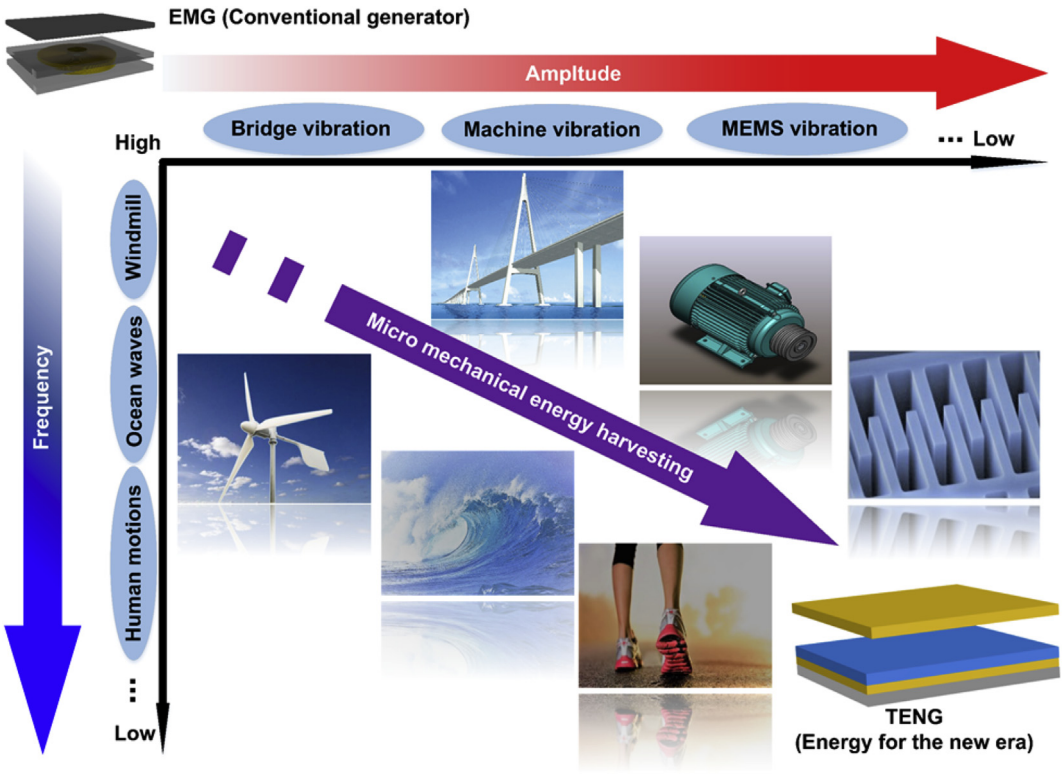

Fig. 5. The prospects of the TENG, which shows remarkable merits than the EMG for harvesting mechanical energy in low-frequency and small-amplitude.

visual demonstration is shown in Video S1. All these results demonstrate the remarkable merit of the TENG than the EMG in harvesting small amplitude vibration energy.

Supplementary data related to this article can be found at https://doi.org/10.1016/j.nanoen.2019.04.047.

Besides the merit of small amplitude, the advantage of the TENG in low frequency has also been verified in Fig. S6, and an overall comparison of EMG and TENG has been summarized in Fig. 4e. To sum up, for the electrical output characteristics, the EMG is approximate to a voltage source with a small impedance in resistive and inductive characteristics. While the TENG can be considered as a current source with a large capacitive impedance. So the EMG has a high short-circuit current but a low open-circuit voltage, while the TENG provides a high open-circuit voltage but a low short-circuit current. For the mechanical energy harvesting characteristics, the TENG is more adept in low frequency and small amplitude, while the EMG in high frequency and large amplitude.

Fig. 5 has shown the prospects of TENG as a milestone in power generation, which has drawn an entirely new pattern for effectively harvesting mechanical energy in two dimensions. Based on the merit in low-frequency, the TENG has huge application potential in the human motions, windmill, ocean waves, and so on. Moreover, it also has a killer application for harvesting mechanical harvesting in small-amplitude, such as the bridge vibration, machine vibration, MEMS vibration, and so on. All these remarkable merits will guide the development prospects of TENG as a foundation of the energy for the new era.

3. Conclusions

In summary, this work presents the effects of the motion amplitude on the output of both the EMG and TENG, which demonstrates that the TENG has a much better performance than that of the EMG at smaller amplitude. Under fixed operation frequency, the maximum open-circuit voltage and short-circuit current of EMG both linearly rise with the increase of the amplitude. While for the TENG, the maximum short-circuit current linearly rise, and the maximum open-circuit voltage grows to saturation. The characteristic differences result that the maximum output power of the TENG rapidly grows to saturation, while that of the EMG grows slowly and gradually. This contrastive characteristic is verified at different frequencies, which has demonstrated that the TENG has dominant scope over the EMG, in not only low-frequency but also small-amplitude. Even at a higher frequency, the TENG also has a dominant scope at small acceleration. For the vibration energy harvesting demonstration, electronics powered by the TENG in small-amplitude has been exhibited and an overall comparison of the TENG and EMG is summarized. Beyond low-frequency, this work has verified the small-amplitude is also a remarkable merit of the TENG for harvesting micro-mechanical energy, which has guided the development prospects of TENG as a foundation of the energy for the new era for internet of things, wearable electronics, robotics and artificial intelligence.

4. Experimental section

4.1. Fabrication process of the EMG

First, an acrylic sheet with the size of 10 × 10 × 2 mm was sandwiched between two pieces of acrylic sheet (60 × 60 × 2 mm) as the frame. Then, a group of copper varnished wire was twined in the frame with 4800 loops as coils. Finally, a neodymium magnet (30 mm in long, 30 mm in width, 10 mm in thick, 35.4 lbs) was assembled. The electricity is produced by the contact-separation between the magnet and Cu coils.

4.2. Fabrication of the TENG

First, an acrylic sheet with the size of 60 × 60 × 2 mm was used as the substrate. Then, a FEP film (60 × 60 mm, thickness of 30 μm), with a Cu electrode (60 × 60 mm, thickness of 40 μm) attached on back side of the FEP film, was pasted onto the substrate. Finally, another Cu film

(60 × 60 mm, thickness of 40 μm) attached on an acrylic (60 × 60 × 2 mm) was used for generating electricity by contact with and separate from the surface of the FEP film.

4.3. Electric measurements

An electrometer (Keithley 6514 system electrometer) was used to measure the output voltages and currents of both generators. Meanwhile, a software platform developed based on LabVIEW was used to record the real-time data. The Electric Measurements has been completed at ~25 °C and ~23%RH.

Conflicts of interest

The authors declare no competing financial interest.

Acknowledgments

The authors gratefully acknowledge the support of the National Key Research and Development Program of China (2016YFA0202704), National Natural Science Foundation of China (No. 61874011), Beijing Talents Foundation (2017000021223TD04), and Beijing Nova Program (No. Z171100001117054). This work also was supported by Major Projects of Science and Technology in Tianjin (No. 18ZXJMTG00020) and the National Natural Science Foundation of China (Grant No. 61671323).

Appendix A. Supplementary data

Supplementary data to this article can be found online at https://doi.org/10.1016/j.nanoen.2019.04.047.

References

[1] T. Someya, Z. Bao, G.G. Malliaras, Nature 540 (2016) 379–385.
[2] W. Gao, S. Emaminejad, H.Y.Y. Nyein, S. Challa, K. Chen, A. Peck, H.M. Fahad, H. Ota, H. Shiraki, D. Kiriya, D.-H. Lien, G.A. Brooks, R.W. Davis, A. Javey, Nature 529 (2016) 509–514.
[3] Z.L. Wang, Nanomater. Energy 58 (2019) 669–672.
[4] F. Xue, L. Chen, L. Wang, Y. Pang, J. Chen, C. Zhang, Z.L. Wang, Adv. Funct. Mater. 26 (2016) 2104–2109.
[5] C. Zhang, Z.L. Wang, Nano Today 11 (2016) 521–536.
[6] Z.W. Yang, Y. Pang, L. Zhang, C. Lu, J. Chen, T. Zhou, C. Zhang, Z.L. Wang, ACS Nano 10 (2016) 10912–10920.
[7] D. Gielen, F. Boshell, D. Saygin, Nat. Mater. 15 (2016) 117–120.
[8] S. Chu, A. Majumdar, Nature 488 (2012) 294–303.
[9] S. Wang, L. Lin, Z.L. Wang, Nano Lett. 12 (2012) 6339–6346.
[10] T. Cheng, Q. Gao, Z.L. Wang, Advanced Materials Technologies, (2019), p. 1800588.
[11] S. Wang, Y. Xie, S. Niu, L. Lin, Z.L. Wang, Adv. Mater. 26 (2014) 2818–2824.
[12] S. Wang, L. Lin, Y. Xie, Q. Jing, S. Niu, Z.L. Wang, Nano Lett. 13 (2013) 2226–2233.
[13] L. Xu, T.Z. Bu, X.D. Yang, C. Zhang, Z.L. Wang, Nanomater. Energy 49 (2018) 625–633.
[14] L.M. Zhang, C.B. Han, T. Jiang, T. Zhou, X.H. Li, C. Zhang, Z.L. Wang, Nanomater. Energy 22 (2016) 87–94.
[15] G.X. Liu, W.J. Li, W.B. Liu, T.Z. Bu, T. Guo, D.D. Jiang, J.Q. Zhao, F.B. Xi, W.G. Hu, C. Zhang, Advanced Sustainable Systems 2 (2018) 1800081.
[16] X. Pu, M. Liu, L. Li, S. Han, X. Li, C. Jiang, C. Du, J. Luo, W. Hu, Z.L. Wang, Advanced Energy Materials 6 (2016) 1601254.
[17] Z.L. Wang, Mater. Today 20 (2017) 74–82.
[18] D.K. Davies, J. Phys. D Appl. Phys. 2 (1969) 1533–1537.
[19] R. Elsdon, F.R.G. Mitchell, J. Phys. D Appl. Phys. 9 (1976) 1445–1460.
[20] T. Guo, G. Liu, Y. Pang, B. Wu, F. Xi, J. Zhao, T. Bu, X. Fu, X. Li, C. Zhang, Z.L. Wang, Extreme Mechanics Letters 18 (2018) 1–8.
[21] F. Xi, Y. Pang, W. Li, T. Jiang, L. Zhang, T. Guo, G. Liu, C. Zhang, Z.L. Wang, Nanomater. Energy 37 (2017) 168–176.
[22] W. Seung, M.K. Gupta, K.Y. Lee, K.-S. Shin, J.-H. Lee, T.Y. Kim, S. Kim, J. Lin, J.H. Kim, S.-W. Kim, ACS Nano 9 (2015) 3501–3509.
[23] L. Zhang, B. Zhang, J. Chen, L. Jin, W. Deng, J. Tang, H. Zhang, H. Pan, M. Zhu, W. Yang, Z.L. Wang, Adv. Mater. 28 (2016) 1650–1656.
[24] J. Zhao, H. Guo, Y.K. Pang, F. Xi, Z.W. Yang, G. Liu, T. Guo, G. Dong, C. Zhang, Z.L. Wang, ACS Nano 11 (2017) 11566–11573.
[25] X.P. Fu, T.Z. Bu, F.B. Xi, T.H. Cheng, C. Zhang, Z.L. Wang, ACS Appl. Mater. Interfaces 9 (2017) 32352–32358.
[26] W. Li, G. Liu, D. Jiang, C. Wang, W. Li, T. Guo, J. Zhao, F. Xi, W. Liu, C. Zhang, Advanced Materials Technologies 3 (2018) 1800189.
[27] Y. Meng, J. Zhao, X. Yang, C. Zhao, S. Qin, J.H. Cho, C. Zhang, Q. Sun, Z.L. Wang, ACS Nano 12 (2018) 9381–9389.
[28] J.M. Wu, Y.H. Lin, B.-Z. Yang, Nanomater. Energy 22 (2016) 468–474.
[29] U. Khan, T.-H. Kim, H. Ryu, W. Seung, S.-W. Kim, Adv. Mater. 29 (2017) 1603544.
[30] L. Jin, W. Deng, Y. Su, Z. Xu, H. Meng, B. Wang, H. Zhang, B. Zhang, L. Zhang, X. Xiao, M. Zhu, W. Yang, Nanomater. Energy 38 (2017) 185–192.
[31] G. Zhu, Y. Su, P. Bai, J. Chen, Q. Jing, W. Yang, Z.L. Wang, ACS Nano 8 (2014) 6031–6037.
[32] J. Chen, J. Yang, Z. Li, X. Fan, Y. Zi, Q. Jing, H. Guo, Z. Wen, K.C. Pradel, S. Niu, Z.L. ACS Nano 9 (2015) 3324–3331.
[33] W. Liu, L. Xu, T. Bu, H. Yang, G. Liu, W. Li, Y. Pang, C. Hu, C. Zhang, T. Cheng, Nanomater. Energy 58 (2019) 499–507.
[34] L. Xu, Y. Pang, C. Zhang, T. Jiang, X. Chen, J. Luo, W. Tang, X. Cao, Z.L. Wang, Nanomater. Energy 31 (2017) 351–358.
[35] T. Jiang, L.M. Zhang, X. Chen, C.B. Han, W. Tang, C. Zhang, L. Xu, Z.L. Wang, ACS Nano 9 (2015) 12562–12572.
[36] C. Zhang, W. Tang, Y. Pang, C. Han, Z.L. Wang, Adv. Mater. 27 (2015) 719–726.
[37] A. Li, Y. Zi, H. Guo, Z.L. Wang, F.M. Fernández, Nat. Nanotechnol. 12 (2017) 481–487.
[38] C.B. Han, T. Jiang, C. Zhang, X. Li, C. Zhang, X. Cao, Z.L. Wang, ACS Nano 9 (2015) 12552–12561.
[39] J. Nie, Z. Ren, J. Shao, C. Deng, L. Xu, X. Chen, M. Li, Z.L. Wang, ACS Nano 12 (2018) 1491–1499.
[40] G. Liu, J. Nie, C. Han, T. Jiang, Z. Yang, Y. Pang, L. Xu, T. Guo, T. Bu, C. Zhang, Z.L. Wang, ACS Appl. Mater. Interfaces 10 (2018) 7126–7133.
[41] C. Zhang, W. Tang, C. Han, F. Fan, Z.L. Wang, Adv. Mater. 26 (2014) 3580–3591.
[42] Y. Zi, H. Guo, Z. Wen, M.-H. Yeh, C. Hu, Z.L. Wang, ACS Nano 10 (2016) 4797–4805.
[43] S. Saadon, O. Sidek, Energy Convers. Manag. 52 (2011) 500–504.
[44] M.R. Bai, G.M. Lin, J. Sound Vib. 198 (1996) 411–427.
[45] S. Takasu, M. Masuda, T. Nishiguchi, A. Kobayashi, CIRP Annals 34 (1985) 463–467.
[46] S. Niu, Z.L. Wang, Nanomater. Energy 14 (2015) 161–192.
[47] S. Niu, S. Wang, L. Lin, Y. Liu, Y.S. Zhou, Y. Hu, Z.L. Wang, Energy Environ. Sci. 6 (2013) 3576.
[48] Y. Zi, S. Niu, J. Wang, Z. Wen, W. Tang, Z.L. Wang, Nat. Commun. 6 (2015) 8376.
[49] B. Zhang, J. Chen, L. Jin, W. Deng, L. Zhang, H. Zhang, M. Zhu, W. Yang, Z.L. Wang, ACS Nano 10 (2016) 6241–6247.
[50] L. Jin, J. Chen, B. Zhang, W. Deng, L. Zhang, H. Zhang, X. Huang, M. Zhu, W. Yang, Z.L. Wang, ACS Nano 10 (2016) 7874–7881.